

## $\delta$ -electron spectroscopy, a tool to study the dynamics of heavy-ion collisions

M. Krämer,\* B. Blank,\* E. Božek,† E. Ditzel, E. Kankeleit,  
G. Klotz-Engmann, C. Müntz, H. Oeschler, M. Rhein, and P. Senger\*

*Institut für Kernphysik, Technische Hochschule, D-6100 Darmstadt, Federal Republic of Germany*

(Received 3 February 1989)

The  $\delta$ -electron spectra from dissipative reactions of the collision systems Pb+U and Pb+Pb show the influence of large nuclear contact with increasing  $Q$  value. An analysis independent of nuclear models allows us to determine the trajectories of the collisions. Comparison with the reaction model of Schmidt, Toneev, and Wolschin and the one of Feldmeier is made. The applicability of  $\delta$ -electron spectroscopy in lighter systems is discussed.

### I. INTRODUCTION

The present paper deals with the investigation of time delay effects in dissipative heavy-ion collisions by means of  $\delta$ -electron spectroscopy. It turns out that in the  $\delta$ -electron production—a complex process involving about 100 electrons—the spectral distribution is sensitive to the dynamics of the collision. This offers a capability to gain insight into the time evolution of the nuclear reaction. Earlier experiments<sup>1,2</sup> already clearly showed the effect of prolonged nuclear collision times on the  $\delta$ -electron and positron spectra. Another experimental approach uses the  $K$  x-ray probabilities measured as a function of energy loss during the collision to extract nuclear contact times.<sup>3</sup> Here the mechanism of lepton production in heavy-ion collisions will only briefly be reviewed since there are several papers<sup>4–6</sup> treating the theoretical description in detail.

The rapidly varying Coulomb field of the two colliding nuclei gives rise to ionization processes from occupied shells into the positive continuum ( $\delta$  electrons). Also, electrons from the lower continuum (Dirac sea) may be excited into vacancies formed earlier in the collision or into the upper continuum, leaving vacancies in the Dirac sea which are observable as positrons. For such one-step processes the scaling model<sup>4,5</sup> predicts a transition amplitude  $a_{if}$  which is essentially the Fourier transform of the quantity  $\dot{R}(t)/R(t)$ .  $R(t)$  is usually the time-dependent internuclear distance and  $\dot{R}(t)$  is the time derivative of this quantity. For a realistic treatment of extended nuclei  $R(t)$  is taken as the root-mean-square radius of the dinuclear charge distribution.<sup>5</sup> Typical  $\dot{R}(t)/R(t)$  curves are shown in the upper part of Fig. 1.

The time-dependent complex amplitude reads

$$a_{if}(t) \propto \frac{1}{\Delta E} \int_{-\infty}^t dt' \frac{\dot{R}}{R}(t') \exp(it'\omega), \quad (1)$$

with  $\omega = \Delta E/\hbar$ , where  $\Delta E = E_e - E_{\text{bind}}$  is the energy transferred to the electron. The typical shape of such spectra for elastic collisions is an exponential function with a decay constant of about one decade per 1 MeV, slightly modified by the energy denominator. Both the scaling model<sup>4</sup> and the coupled-channels formalism<sup>6</sup>

reproduce the shape of the measured spectra. Only the coupled-channels calculations predict absolute cross sections which reproduce the experimental yield within a factor of 2. These calculations include multistep processes and use the exact transition matrix elements.

In Fig. 1 (mid part) the transition amplitude  $a_{if}(t)$  is plotted in the complex plane. The quantity relevant for  $\delta$ -electron production is the distance between the points for  $t = \pm\infty$ . In case of elastic scattering (dashed lines) the real part vanishes because of the symmetry of  $\dot{R}(t)/R(t)$  around  $t=0$  (see Fig. 1, upper left part).

For dissipative collisions a schematic “atomic-clock” model<sup>6</sup> may be established: the nuclei approach each other on Rutherford trajectories, stick together for a contact time  $\tau_{\text{atomic}}$  with radial velocity  $\dot{R}=0$ , and separate again following Rutherford trajectories. This situation is shown by the solid curves in Fig. 1. The phase shift  $\Delta\Phi = \omega\tau_{\text{atomic}}$  gives rise to destructive interference between the incoming and outgoing part of  $a_{if}(t)$ , leading to pronounced minima in the  $\delta$ -electron spectra. The extinction would be perfect if there was no energy loss in the reaction. Instead, the difference in height of incoming and outgoing  $\dot{R}(t)/R(t)$  washes out the interference pattern resulting in a broad minimum as exhibited by the solid curve in the lower left part of Fig. 1. In comparison with the elastic case one can expect deviations up to an order of magnitude which should provide a good signature for nuclear contact. In the earlier experiments<sup>1,2</sup>  $\delta$ -electrons were measured up to 1.5 MeV, only. One observed a steeper descent than expected for elastic scattering.

For a realistic treatment of the nuclear collision problem several reaction models exist. We have constrained ourselves to the model of Schmidt, Toneev, and Wolschin<sup>7</sup> (STW) and the one of Feldmeier<sup>8</sup> which seem to be best suited for very heavy-ion collisions.

The STW model considers the nuclei as “hard spheres” but a correction to account for the deformed shapes in the exit channel is applied. The motion is calculated from macroscopic equations including friction with large coefficients fitted to experimental data. Its predictions for nuclear trajectories come close to the atomic-clock model visible also in the corresponding  $\delta$ -electron spectra

(Fig. 1).

The Feldmeier model also uses macroscopic variables, but friction coefficients evolve from interaction between macroscopic and microscopic degrees of freedom. Further, the nuclei are allowed to deform and especially in the outgoing phase a pronounced neck can develop leading to smooth trajectories and prolonged interaction times. This behavior manifests itself in the  $\delta$ -electron spectrum exhibiting a smooth minimum shifted towards lower electron energies (Fig. 1, lower right part).

As an illustration, Fig. 2 shows the nuclear interaction times  $\tau_{\text{nuclear}}$ , defined as the time between contact and

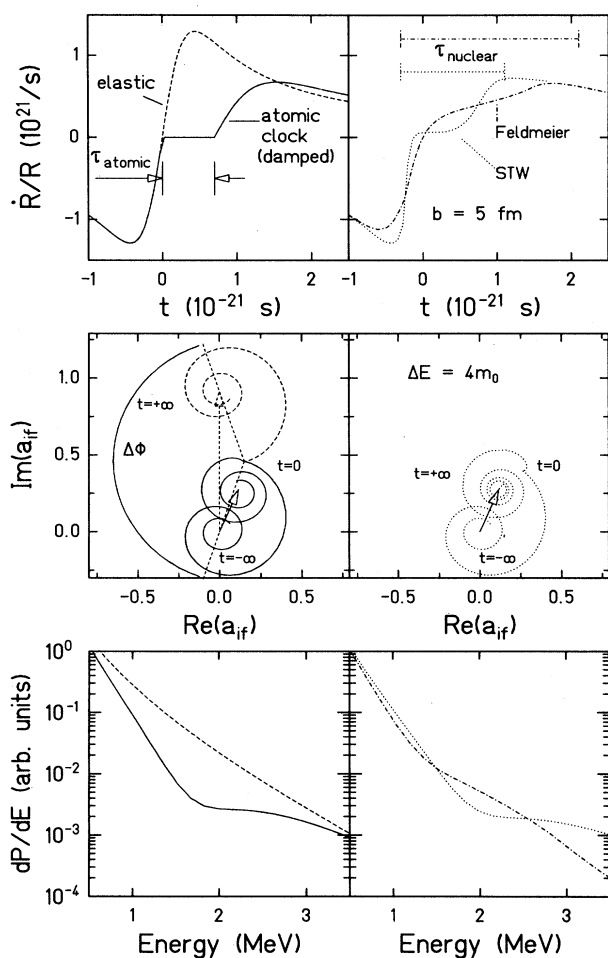


FIG. 1. Illustration of the influence of various trajectories on the  $\delta$ -electron spectra calculated within the scaling model for the reaction Pb+Pb at 8.6 MeV/nucleon at an impact parameter of 5 fm. Upper part:  $\dot{R}(t)/R(t)$  as a function of time. Middle part: time-dependent transition amplitudes for an energy transfer of  $\Delta E = 4m_0$ . A situation is shown where the phase shift  $\Delta\Phi$  leads to maximum destructive interference. On the right-hand side the amplitude only for the STW model is given evidencing its similarity with the atomic-clock concept. Lower part:  $\delta$ -electron spectra corresponding to the trajectories in the upper part.

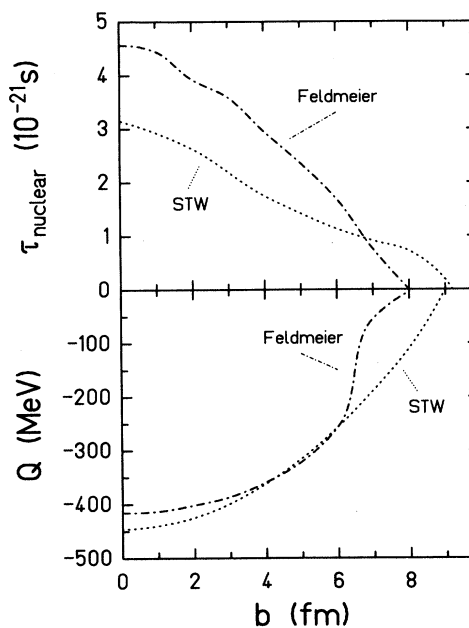


FIG. 2. The nuclear interaction times  $\tau_{\text{nuclear}}$  and the  $Q$  values predicted by two models are given as a function of impact parameter for the reaction Pb+Pb at an incident energy of 8.6 MeV/nucleon.

rupture as a function of the impact parameter for the reaction Pb+Pb at 8.6 MeV/nucleon. The predictions of the two models differ strongly. The neck formation in the Feldmeier model results in a much longer contact. The  $\delta$ -electron emission, however, is only sensitive to the variation of the monopole part of the Coulomb potential. Therefore, nuclear interaction times as defined are only a crude estimate and trajectories  $R(t)$  or better  $\dot{R}(t)/R(t)$  curves should be compared. The  $Q$  values predicted by these models are also given in Fig. 2.

The present paper is organized as follows. First the experimental device and the analysis procedure is outlined. The main section presents the measured  $\delta$ -electron spectra from the collision systems Pb+U and Pb+Pb together with reaction model predictions. The most detailed information on the trajectories of dissipative collisions are obtained by an analysis independent from reaction models, as already reported in Ref. 18. Within this part the predictions of the two models mentioned are discussed. Further on, the applicability of  $\delta$ -electron spectroscopy for the study of collision dynamics in lighter systems is discussed.

## II. EXPERIMENT

The experiments were performed at the UNILAC accelerator of GSI, Darmstadt. About  $10^{11}$   $^{208}\text{Pb}$  ions per s were impinging on self-supporting or C-backed  $^{208}\text{Pb}$ ,  $^{238}\text{U}$ ,  $^{169}\text{Tm}$ , and  $^{108}\text{Pd}$  targets of  $\approx 400 \mu\text{g}/\text{cm}^2$  thickness. The experimental device was the TORI spectrometer.<sup>9</sup> This apparatus is an S-shaped magnetic transport system

designed to measure simultaneously electrons and positrons with energies up to 3 MeV, as well as scattered heavy ions, with high efficiency. A schematic view of the apparatus is depicted in Fig. 3, considered as an S-shaped solenoid. The field strength on the central line (shown as an inset) is higher at one end of the spectrometer to create a magnetic mirror. The toroidal configuration produces an inhomogeneous field resulting in a drift of the leptons in opposite directions according to the sign of their charge. The separation of positrons from electrons is absolutely necessary because of the  $10^4$  times higher yield of the latter. The drift reaches its maximum value after the first quarter torus where the electrons are detected in cooled Si(Li) counters or stopped by a semi-circular diaphragm. The electron counters were placed to detect preferentially the electrons of higher energies and to avoid a pileup of the much more frequent low-energetic ones. The positrons pass through the open half and are focused back onto the central line in the second quarter torus. Their energy was measured in a liquid-nitrogen cooled Si(Li) diode of 5 cm diameter and 5 mm depletion depth. A surrounding fourfold segmented NaI-ring crystal detects the 511 keV annihilation radiation. Operating in sum mode at least one 511 keV quantum in coincidence with a signal from the diode is requested to accept a positron event.

All lepton counters were calibrated in energy and response function using conversion lines from the isotopes  $^{113}\text{Sn}$  (365 keV) and  $^{207}\text{Bi}$  (481 and 975 keV). In addition the  $\beta$  sources  $^{68}\text{Ge}$ ,  $^{22}\text{Na}$ , and  $^{90}\text{Sr}$  were used. To

verify the obtained response functions, especially for positrons for which no natural monoenergetic source exists, the measurement of the pair conversion of the  $0^+ \rightarrow 0^+$  transition in  $^{90}\text{Zr}$  (1750 keV) is favorable. The spectrum of the sum of the lepton energies is shown in Fig. 4. It is reproduced by the dyadic product of the response functions.

In order to determine the contribution of leptons of nuclear origin the  $\gamma$ -ray spectrum was measured in a  $7.6 \times 7.6$  cm NaI or in a  $10.2 \times 15.2$  cm  $\text{BaF}_2$  crystal. The  $\gamma$  detector was mounted in  $90^\circ$  direction with respect to the beam axis leading to maximum Doppler broadening but no Doppler shift. The advantage of the  $\text{BaF}_2$  crystal, compared with a  $7.6 \times 7.6$  cm NaI, is a three to four times larger peak efficiency for  $\gamma$  radiation of about 2 MeV and a better timing resolution, its intrinsic value being less than 1 ns. The good timing is an important parameter in order to separate prompt  $\gamma$  rays from neutron-induced background by time of flight. Figure 5 shows measured and calculated response functions.

Position-sensitive heavy-ion counters were used to measure the angles of the outgoing fragments and to distinguish fission events from elastic scattered heavy ions. That was provided by PPAC's working with delay lines. They cover laboratory angles between  $14^\circ$  and  $76^\circ$ . Two types of PPAC's were used either with strips of constant polar angles  $\theta$  and an angular resolution  $\Delta\theta \approx 2^\circ$  (experiments Pb+U and Pb+Tm) or with  $x$ - $y$  grids having a position resolution of  $\Delta x = \Delta y = 1$  mm or  $\Delta\theta \approx 1.5^\circ$ ,  $\Delta\phi \approx 2^\circ$  (Pb+Pb, Pb+Pd). Due to the small distance be-

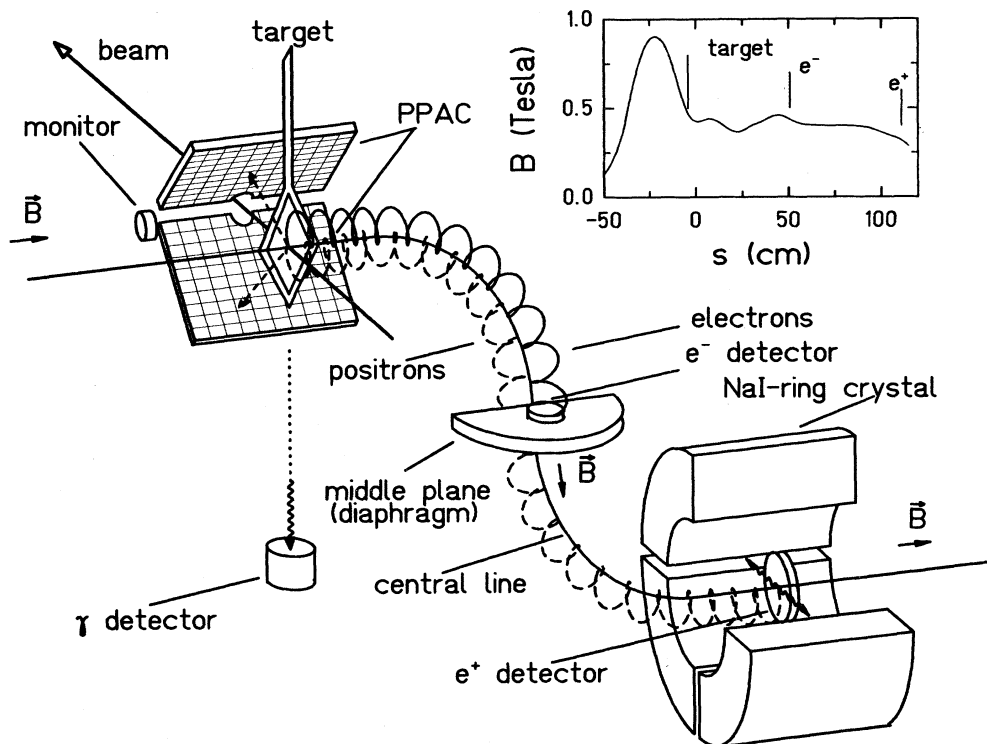


FIG. 3. Display of the TORI spectrometer, showing the detector arrangement (note in corresponding size). The magnetic field strength along the central line is shown as an inset. In addition, the position of the detectors is indicated.

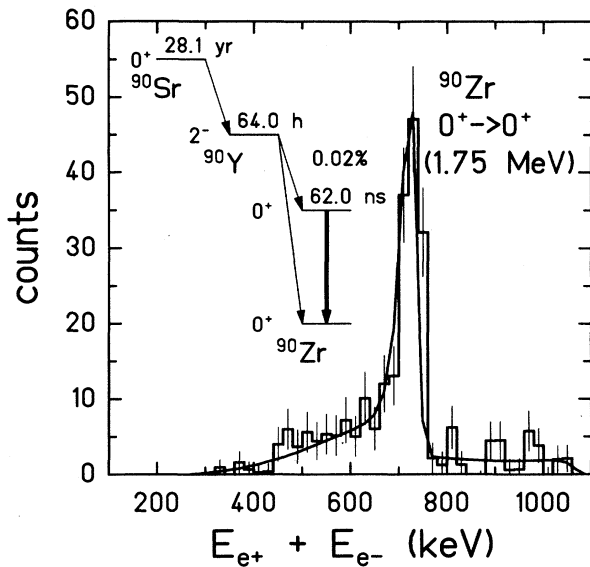


FIG. 4. Pair conversion of the  $0^+ \rightarrow 0^+$  transition in  $^{90}\text{Zr}$ . Histogram: Measured sum spectrum of the lepton kinetic energies. Solid curve: coincidence response function of  $e^+$  and  $e^-$  detector, scaled in height to account for the angular correlation of an  $E0$  transition.

tween target and PPAC of about 5.5 cm the resolution is limited by the beam-spot size of  $\approx 3$  mm.

Both types of PPAC's are equipped with a double readout of the delay lines allowing for double-hit recognition in cases of sequential fission. Figure 6 illustrates the method of separation of fission events. The two signals from each delay line are plotted versus each other. For a single hit the sum of both time signals must be a constant

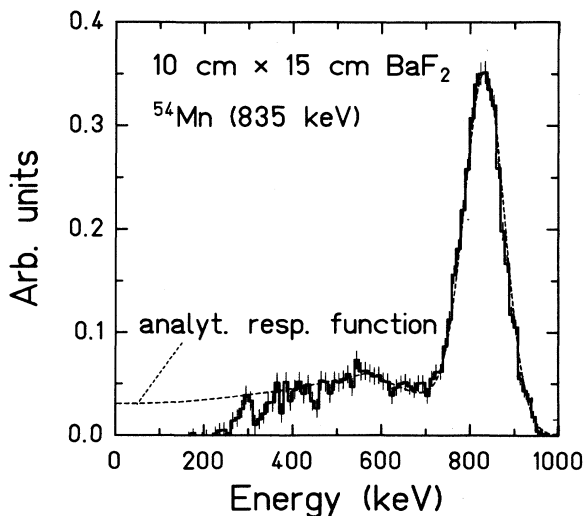


FIG. 5. Measured  $\gamma$  spectrum of a 835 keV  $\gamma$  source in the  $\text{BaF}_2$  scintillator together with the analytic response function (dashed curve).

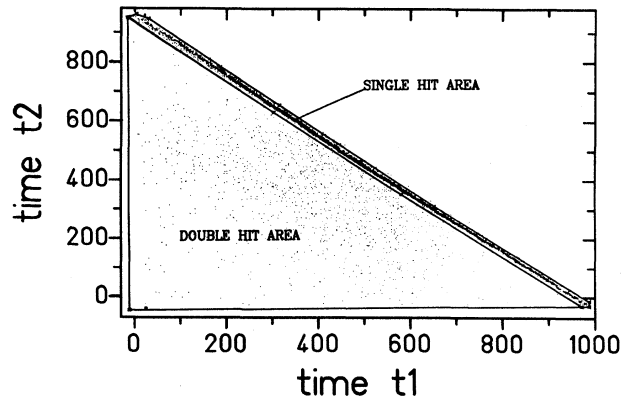


FIG. 6. Separation of fission events by plotting the time signals from each end of a delay line. Single hits give a constant sum of the two time values (diagonal line).

equal to the total delay time. Such events appear on a diagonal line (see Fig. 6). If two fission fragments enter the counter then only the first signal is read at each end of the delay line and the sum is less than the total delay time. These events appear in the triangular area below the constant sum line. In addition the energy-loss signal from each counter was used to discriminate single fission fragments hitting the counter. The energy-loss signals of such events are smaller than those from a heavy collision partner or from two fission fragments entering the PPAC simultaneously.

### III. DATA ANALYSIS

#### A. Reaction classes and $Q$ value determination

For the systems and beam energies investigated in the current experiments one expects dissipative reactions down to a  $Q$  value of  $-400$  MeV. For nuclei heavier than lead such an excitation causes fission with a probability close to one. The fission process is sequential<sup>10</sup> and takes place several  $10^{-20}$  s after the collision. Therefore, a well-defined primary scattering angle exists. The influence of sequential fission on the production of  $\delta$  electrons is negligible.<sup>11</sup> Depending on  $Q$  value and mass of the nuclei involved, either both partners fission (four-body events), one survives (three-body events), or both survive (binary events, including elastic scattering). This number of outgoing fragments characterizes three reaction classes.

For fission events the primary scattering angle has to be reconstructed. This is done by averaging the angles or Cartesian coordinates of the single fission fragments. Because their masses and velocities are not known this method yields the correct angles only on the average. For a purely polar-angle sensitive counter an additional source of uncertainty is the possibility of out-of-plane fission.

The  $Q$ -value determination is performed by geometrical considerations. Due to the small distance between

target and PPAC, there is no way to measure the time of flight with sufficient accuracy. The conservation of energy and momentum in the laboratory system assuming zero mass transfer yields

$$Q = E_P \left[ \frac{A_P \sin^2 \vartheta_P + A_T \sin^2 \vartheta_T}{A_T \sin^2 (\vartheta_P + \vartheta_T)} - 1 \right], \quad (2)$$

where  $E_P$  denotes the beam energy and the subscripts  $P$  and  $T$  refer to projectile and target, respectively. For symmetric systems this corresponds to the deviation of the sum of the primary scattering angles from  $90^\circ$  in the laboratory system.

For binary reactions the targetlike partner is identified through its larger laboratory angle in the PPAC pair. In case of fission events, projectilelike and targetlike partners are identified through the assumption that the heavier one always should undergo fission. This is reasonable because the fission probability of excited nuclei rises very steeply with increasing mass.

The combined uncertainty of all these effects was estimated with the aid of Monte Carlo (MC) calculations. They show that the  $Q$ -value resolution for binary events is of the order of 100 MeV. For three-body events the resolution is worse and the measured  $Q$  value has to be corrected for systematic errors by up to 100 MeV. Four-body events cannot be subdivided into  $Q$ -value regions due to lack in resolution.

In view of the statistical fluctuations of  $\approx 100$  MeV inherent in heavy-ion reactions,<sup>8</sup> little is gained by improved  $Q$  resolution far below 100 MeV.

In order to have a trigger for the various impact parameter regimes and hence certain trajectories one plots the  $Q$  value versus the laboratory scattering angle  $\vartheta$  of one fragment. For three-body events the angle of the nonfissioning partner is to be preferred to avoid the systematic error of angular averaging. Certain regions of impact parameter  $b$  were selected by placing windows in the  $Q$ - $\vartheta$  distribution. Figure 7 shows this distribution for the system Pb+Pb together with the selected windows.

The impact parameters associated with the  $Q$  windows were deduced from Monte Carlo simulations of the reaction kinematics.<sup>12</sup> These calculations are based on a  $Q(b)$  dependence taken from Ref. 7. To account for the nuclear forces, a deflection function of the form<sup>13</sup>

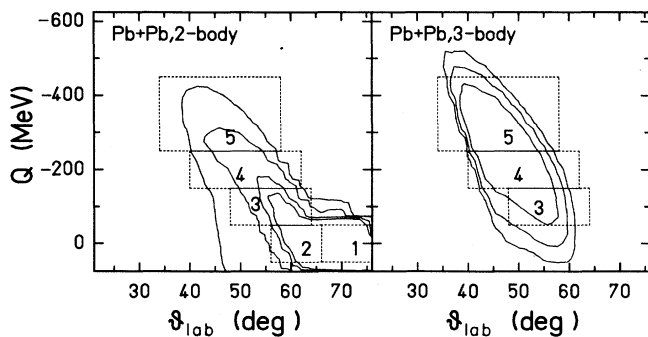


FIG. 7.  $Q$  value vs laboratory angle of surviving leadlike nucleus for the reaction Pb+Pb at 8.6 MeV/nucleon.

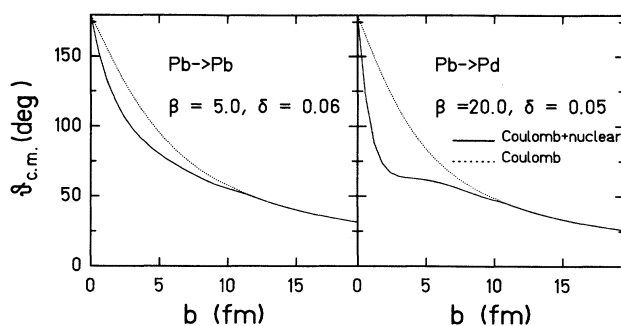


FIG. 8. Deflection functions for the systems Pb+Pb and Pb+Pd used in the Monte Carlo calculations. The parameters  $\beta$  and  $\delta$  are explained in the text.

$$\vartheta(b) = \vartheta(b)_{\text{Coulomb}} + \vartheta(b)_{\text{nuclear}}, \quad (3)$$

with

$$\vartheta(b)_{\text{nuclear}} = -\beta \left( \frac{\delta}{\beta} \right)^{b/b_{\text{graz}}} \frac{b}{b_{\text{graz}}} \vartheta_{\text{graz}} \quad (4)$$

was used. The parameter  $\delta$  is responsible for the deviation from Coulomb trajectories near the grazing angle, while  $\beta$  controls the focusing behavior at smaller impact parameters. Both parameters are generally related to the kinetic energy above the Coulomb barrier.<sup>13</sup> For the systems under study they were adjusted to yield the measured  $Q$ - $\vartheta$  distributions. As can be seen from Fig. 8 the deflection function for Pb+Pb is Coulomb-like, while for Pb+Pd the nuclear attraction competes strongly with the Coulomb repulsion. For a realistic description of the fission events, mass diffusion, and fission probabilities based on experimental data<sup>14</sup> are included.

Leptons and  $\gamma$  rays were analyzed simultaneously under the kinematical constraints mentioned above, normalized to the heavy-ion counting rate to yield the probability per collision and corrected for the appropriate detector response functions.

## B. Leptons from internal conversion

Before electron spectra can be interpreted the contribution from internal pair conversion has to be subtracted. An essential effort of the analysis is the determination of this part. To achieve this the unfolded  $\gamma$ -ray spectra are converted into electrons and positrons using the theoretical double-differential pair conversion coefficients of Ref. 15 and the electron conversion coefficients of Ref. 16. The assignment of multiplicities is done in analogy to Ref. 2. The high-energy part above  $\approx 1.5$ – $2.0$  MeV contains predominantly statistical  $E1$  transitions and is described by the function

$$\frac{dN}{dE_\gamma} = \left( \frac{E_\gamma}{P_3} \right)^{P_1/P_2} \exp \left( \frac{-E_\gamma}{P_2} \right), \quad (5)$$

where  $P_1$  defines the position of the maximum ( $\approx 1.2$  MeV),  $P_2$  may be considered as a temperature (usually

$\approx 400\text{--}600$  keV),  $P_3$  serves as a height parameter. In the low-energetic part of the spectrum a surplus remains which is assumed to be of  $E2$  multipolarity [see Fig. 9(a), two-body events]. To account for the nuclear charges entering in the calculation of the conversion coefficients the  $\gamma$  radiation has been weighted in the following way: three-body,  $Z=82$ , 30% and  $Z=46$  or  $41$ , 70%; four-body,  $Z=46$  or  $41$ , 50% each.

The multipolarity assignment can be verified with the aid of the simultaneously measured positron spectra. For the dissipative collision system with  $Z_P + Z_T = Z_{\text{united}} \leq 174$  studied in this paper the contribution from nuclear positrons dominates ( $\approx 80\%$  for Pb+U and  $> 90\%$  for Pb+Pb). This is due to the fact that the production probability for atomic positrons increases as  $\approx Z_{\text{united}}^{19}$  for the considered  $Z$  range.<sup>17</sup> For comparison with the measured positron spectra the calculated atomic<sup>6</sup> and nuclear contributions are added. As one can see in Fig. 9(b) the agreement between measured and calculated positron spectra is quite good. It turns out, that for three-body events an additional admixture of  $E2$  also for

$\gamma$  energies around 2 MeV is necessary to reproduce the measured positron distribution [Fig. 9(b)]. The multipolarity mixing used so far would give an overestimation of positron yield by a factor of up to 40%. This is probably due to deexcitation of fission products in the Nb-Pd region and a similar situation is encountered in the case of binary Pb+Pd collisions where also large  $E2$  contributions have to be taken into account. The measured electron spectra and the fraction from conversion processes are shown in Fig. 9(c). This fraction increases with  $Q$  value and amounts up to 50%. The systematic uncertainty of the electron yield from conversion using this method of multipolarity verification is estimated to be about 15%. The same procedure gives consistent results when applied to medium-heavy systems (Fig. 14).

#### IV. RESULTS AND DISCUSSION

##### A. The system Pb+U

The system Pb+U was investigated at 8.4 MeV/nucleon beam energy. Because uraniumlike nuclei very

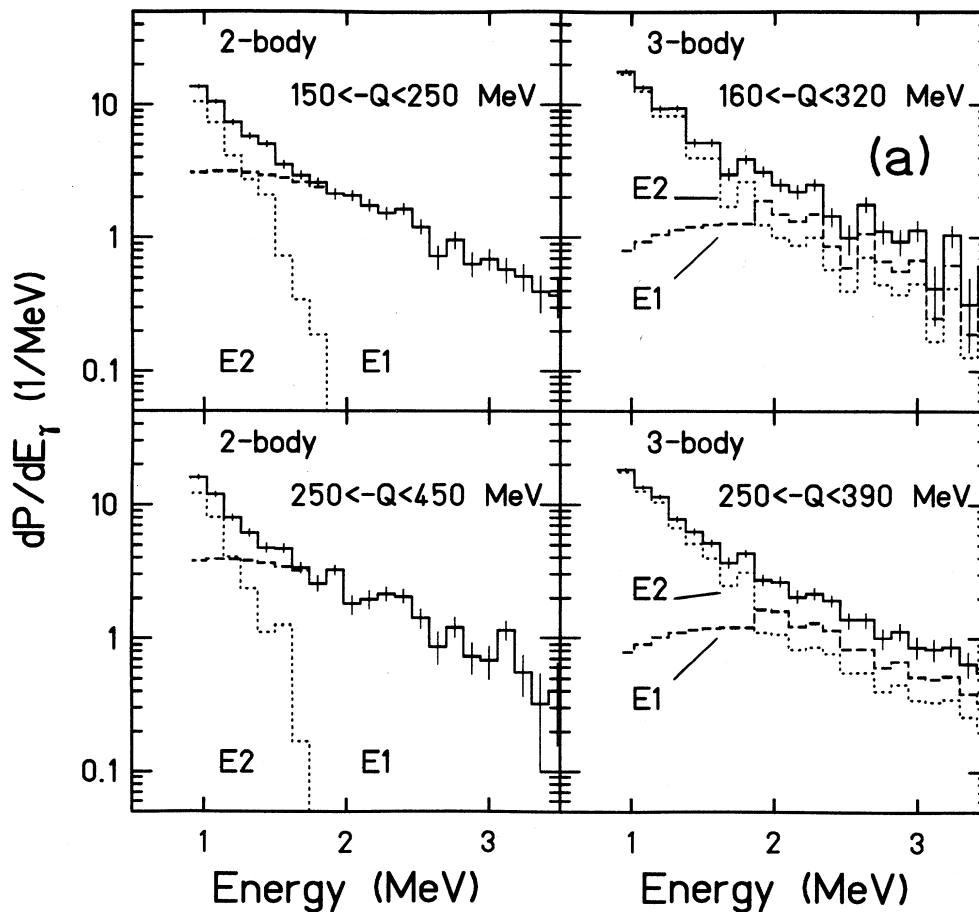


FIG. 9. Method of nuclear background determination for Pb+Pb at 8.6 MeV/nucleon. (a) Measured  $\gamma$  spectra (solid histograms) together with the assumed multipolarity decomposition ( $E1$ , dashed;  $E2$ , dotted). (b) Measured positron spectra (histograms) compared with calculated nuclear contribution (dashed curve). The solid curve is the sum of nuclear and atomic contributions. The good agreement confirms the multipolarity assignment. (c) Measured electron spectra (histograms) with the calculated conversion contribution.

likely undergo fission already at small excitation energies, dissipative collisions lead nearly always to three-body or four-body events. In the first case, with negligible mass transfer, the leadlike nucleus survives. In case of four-body reactions one can suppose mass transfer from uranium to lead since the fission probability increases rapidly only for  $Z > 85$ .<sup>14</sup> The fission of leadlike nuclei as well as mass transfer are necessarily correlated with large energy loss. Four-body events therefore represent a reaction class with high  $Q$  values, on the average  $Q \approx -260$  MeV.

Figure 10 shows the  $\delta$ -electron spectra (histograms) after subtraction of nuclear contributions. The effect of longer nuclear contact with increasing energy loss is clearly seen. The spectra show a steeper descent for electron energies less than 1.5 MeV and a dip is formed around 1.7 MeV. For higher electron energies the spectra flatten.

The solid curves in Fig. 10 are coupled-channels calculations based on trajectories from the reaction model of Ref. 7. They are weighted with the impact parameter distributions indicated as insets in the figure. The distributions are obtained from a Monte Carlo simulation of the kinematics of the reaction Pb+U. The dashed curves in Fig. 10 represent the calculated spectra assuming

Rutherford trajectories and the same impact parameter distributions.

In the STW model the correlation between  $Q$  value and impact parameter  $b$  is unique. The width of the  $b$  distributions is therefore determined only by the experimental conditions. The relatively narrow distribution for the four-body events is a consequence of the small  $Q$  window in which four-body fission occurs and of the angular acceptance of our counter setup for this reaction class.

Concerning the shape of the spectra one finds general agreement between theory and experiment. To match the absolute height, however, factors of 1.3 and 1.6 are necessary. These findings are in accordance with earlier results for the system U+U (Refs. 1 and 2) where the theory also underestimates the experiment.

The spectra to four-body events do not differ significantly from those of three-body events with similar  $Q$  value. Because of the presumed mass transfer correlated with four-body events one could expect that contact times are longer. Our conclusion is that the mass transfer of  $\Delta A \approx 13$  units estimated from the element distributions in Ref. 14 does not influence the spectra.

Also, due to the narrow  $Q$  region selected the minimum should be more pronounced. However, in the

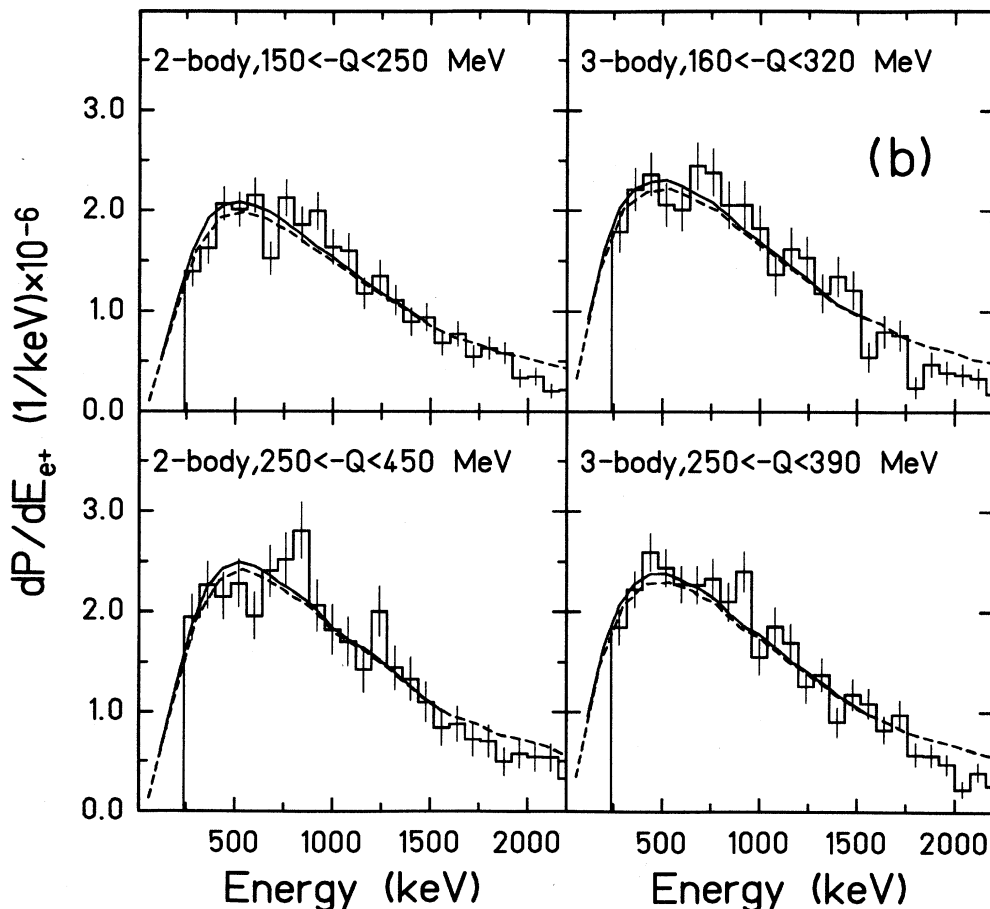


FIG. 9. (Continued).

STW model the correlation  $\tau(b)$  between contact time  $\tau$  and impact parameter  $b$  is unique. More realistic is a distribution of contact times for a fixed impact parameter. In spite of the fact that this is not accounted for in the calculations, the experimental width in  $b$  is sufficient to reproduce the shape of the spectra from central-collision three-body events. As a consequence the intrinsic fluctuations must be smaller than the experimental  $b$  resolution.

The situation is different for four-body events. For this reaction class theory can only be matched with experiment if the width of the  $b$  distribution  $\Delta b_{\text{expt}}$  is increased artificially by 50% to  $\Delta b_{\text{broadened}}$ . This additional width can be attributed to intrinsic fluctuations of the contact time  $\tau(b)$ :

$$\Delta\tau_{\text{intrinsic}} = \left[ \left( \frac{\partial\tau}{\partial b} \Delta b_{\text{broadened}} \right)^2 - \left( \frac{\partial\tau}{\partial b} \Delta b_{\text{expt}} \right)^2 \right]^{1/2}, \quad (6)$$

where  $\partial\tau/\partial b$  is taken from the STW model. The relative size of these fluctuations was estimated to  $\Delta\tau/\tau \approx 1$ . We emphasize, however, that this estimation is based on mean trajectories as predicted by the STW model. All

statements concerning fluctuations require the definition of a mean value and, therefore, are model dependent

### B. The system Pb + Pb

Using three-body events as trigger for dissipative collisions has the disadvantage of low- $Q$  resolution, caused by the uncertainty inherent in the averaging of fission fragment angles and neglect of mass transfer. Therefore, the investigations were continued with the system Pb + Pb at 8.6 MeV/nucleon. In this reaction one can expect binary collisions with high  $Q$  value which can be determined with much better resolution. No angular averaging is needed and furthermore, neglecting of mass transfer is justified. Reactions involving mass transfer result in one partner heavier than lead and such nuclei likely undergo fission<sup>14</sup> and hence are observed as three-body events. Very rare four-body events are seen, too. Yet their yield is too low to obtain statistically significant electron spectra.

Figure 11 shows the experimental spectra (histograms) after subtraction of nuclear contributions. To be consistent with the method of trajectory determination discussed in Sec. IV C the scaling model<sup>4,5</sup> is used to com-

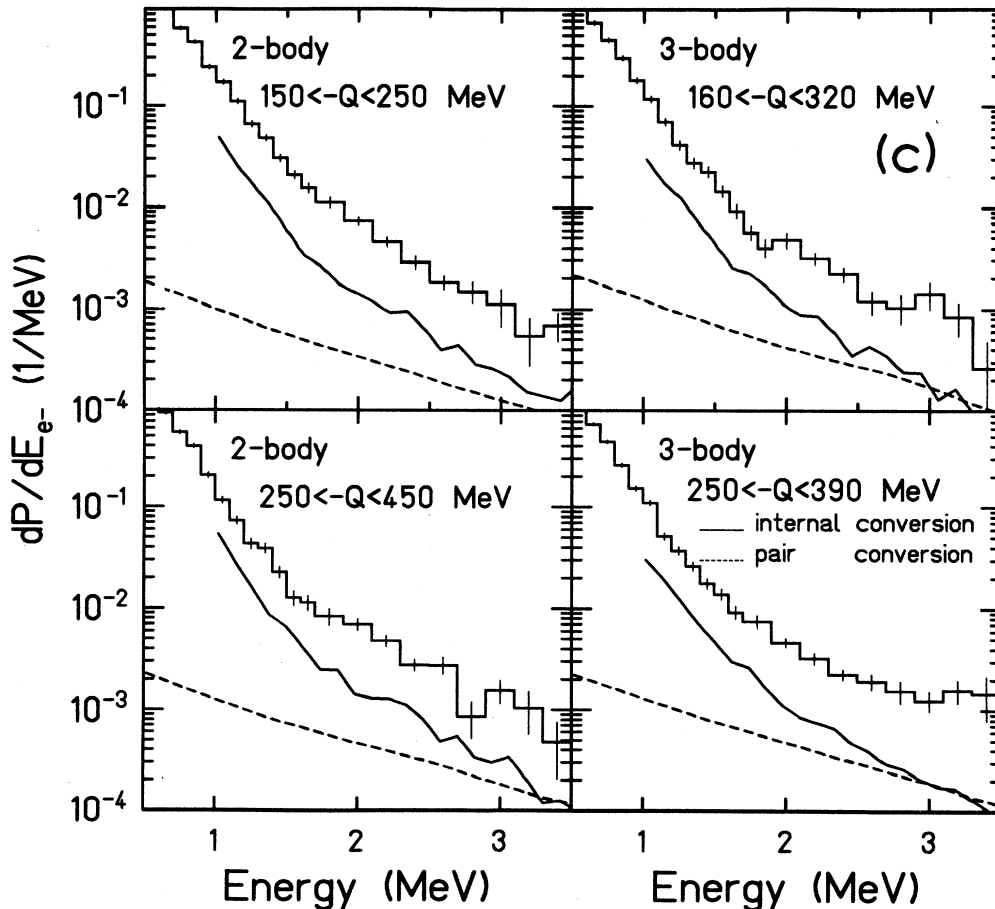


FIG. 9. (Continued).

pare experiment with reaction model predictions. The solid curves in Fig. 11 represent calculations with trajectories according to the STW model. The absolute height is determined to match the spectra at low energies. The appropriate impact parameter distributions obtained by MC simulations are indicated in the insets. The dashed lines are computed spectra with Rutherford trajectories. Comparing the calculations for elastic scattering with the

experiment one clearly recognizes the increasing effect of nuclear contact with increasing energy loss. Similar to the case Pb+U a dip around 1.6 MeV appears for the largest energy loss. The theory curves for deep-inelastic collisions agree rather well with experiment, although improvements should be envisaged.

One should mention that coupled-channels calculations using STW trajectories reproduce the shapes of the ex-

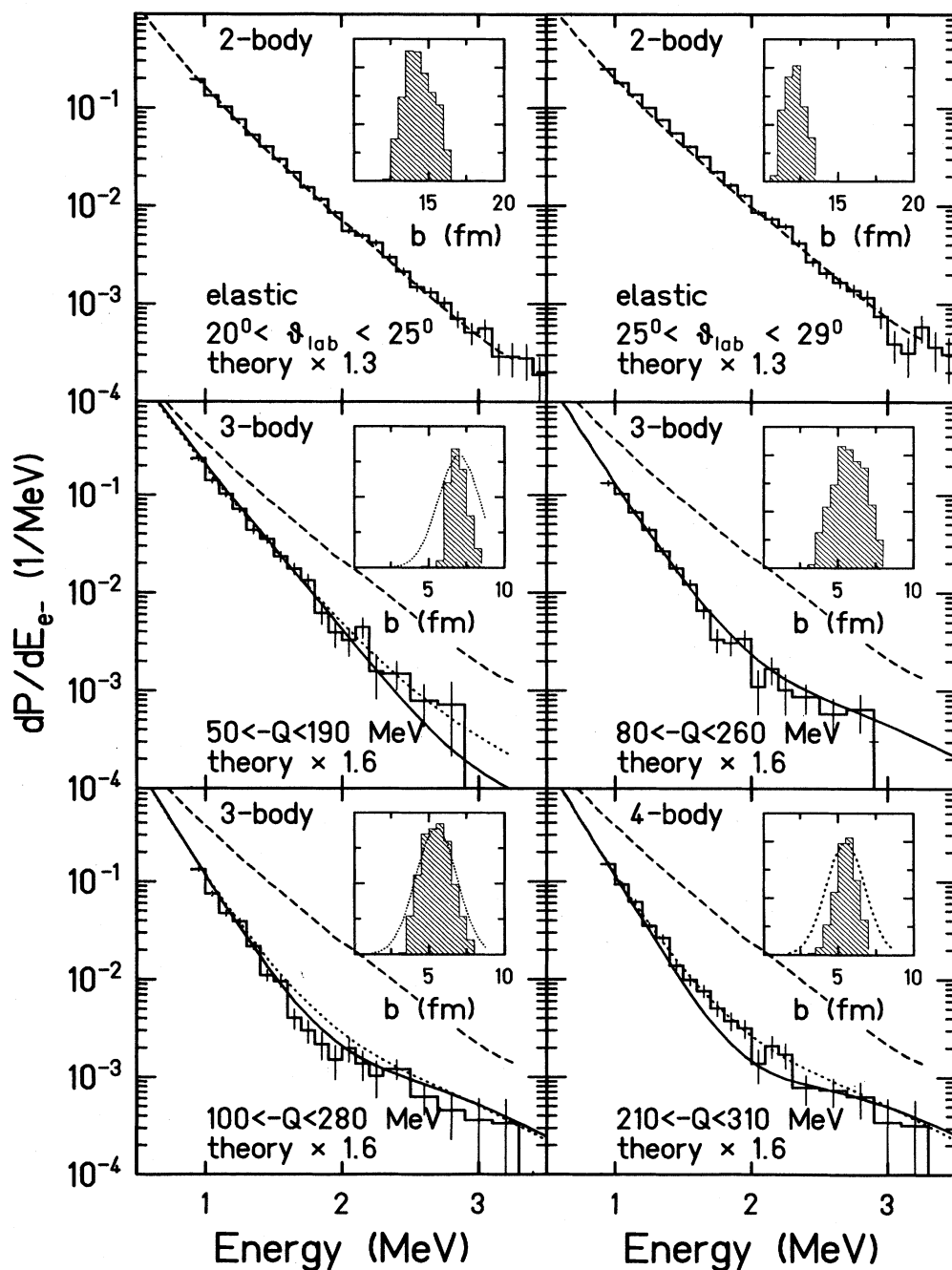


FIG. 10. Comparison of measured  $\delta$ -electron spectra (histograms) from Pb+U at 8.4 MeV/nucleon with coupled-channels calculations (Ref. 11). Solid curves: with STW trajectories; dashed curves: with Rutherford trajectories, both weighted with the impact parameter distributions shown as insets. The dotted curves are the results of a broadened  $b$  distribution to estimate fluctuations.

perimental spectra for elastic and three-body events. For binary collisions, especially those with the largest energy loss, the dip around 2 MeV is more pronounced than in the experiment. Normalization factors between 1.8 and

2.2 are needed for elastic and dissipative collisions, respectively.

Comparing the  $\delta$ -electron spectra for the two systems Pb+Pb and Pb+U in similar  $Q$ -value regimes one does

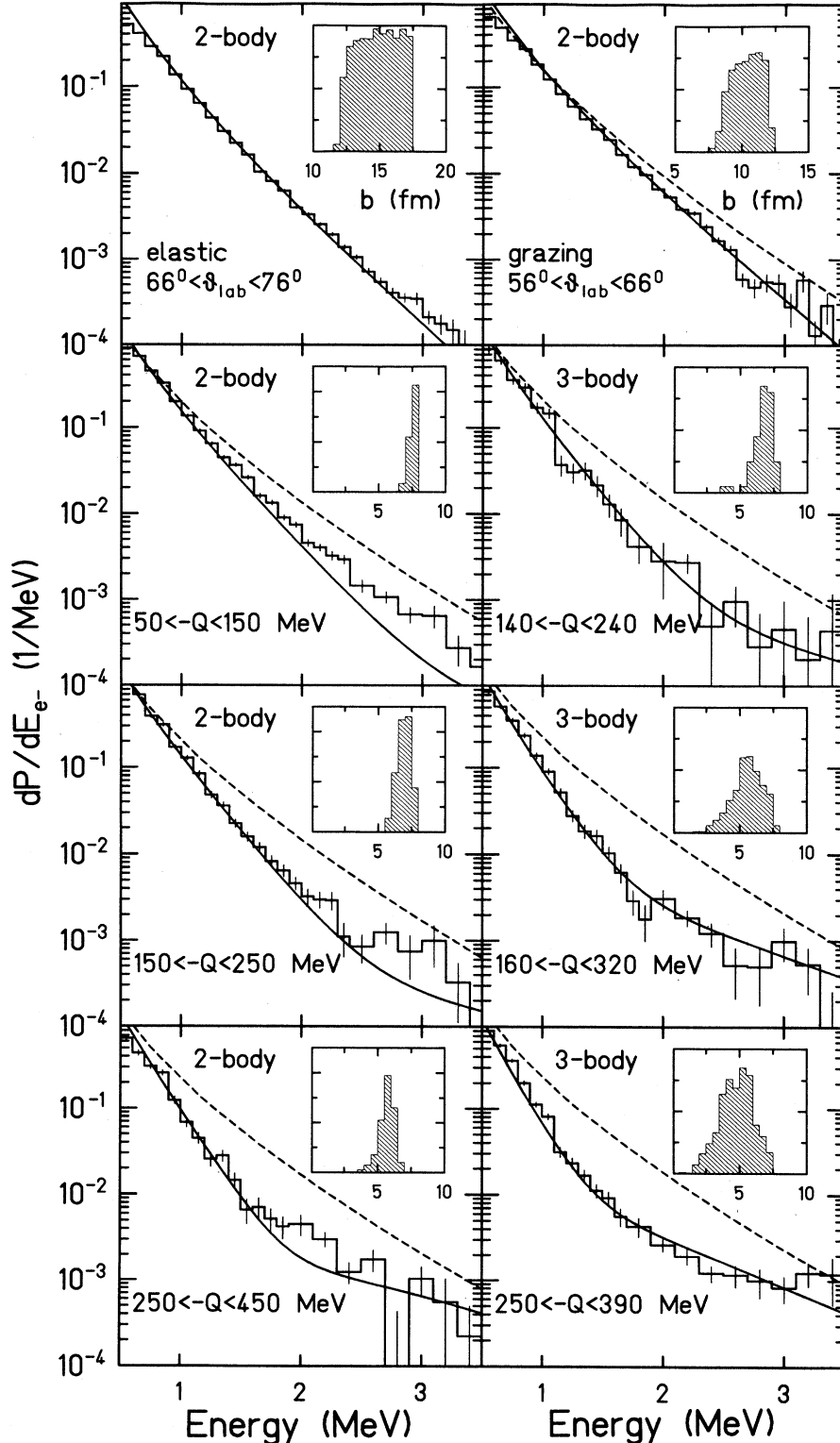


FIG. 11. Comparison of  $\delta$ -electron spectra of the reaction Pb+Pb at 8.6 MeV/nucleon with scaling model predictions based on Rutherford trajectories (dashed lines) and based on STW trajectories (solid lines) weighted with the  $b$  distributions (insets).

not find significant deviations beyond the experimental uncertainties. This can be explained in the framework of the STW model in which the mean values of contact times are expected to differ only by  $\approx 20\%$ . Dealing with

fluctuations of the order  $\Delta\tau/\tau \approx 1.0$  such fine differences are not appreciable.

A further comparison can be made with the results reported in Ref. 19.  $\delta$  electrons from the system U+Au at

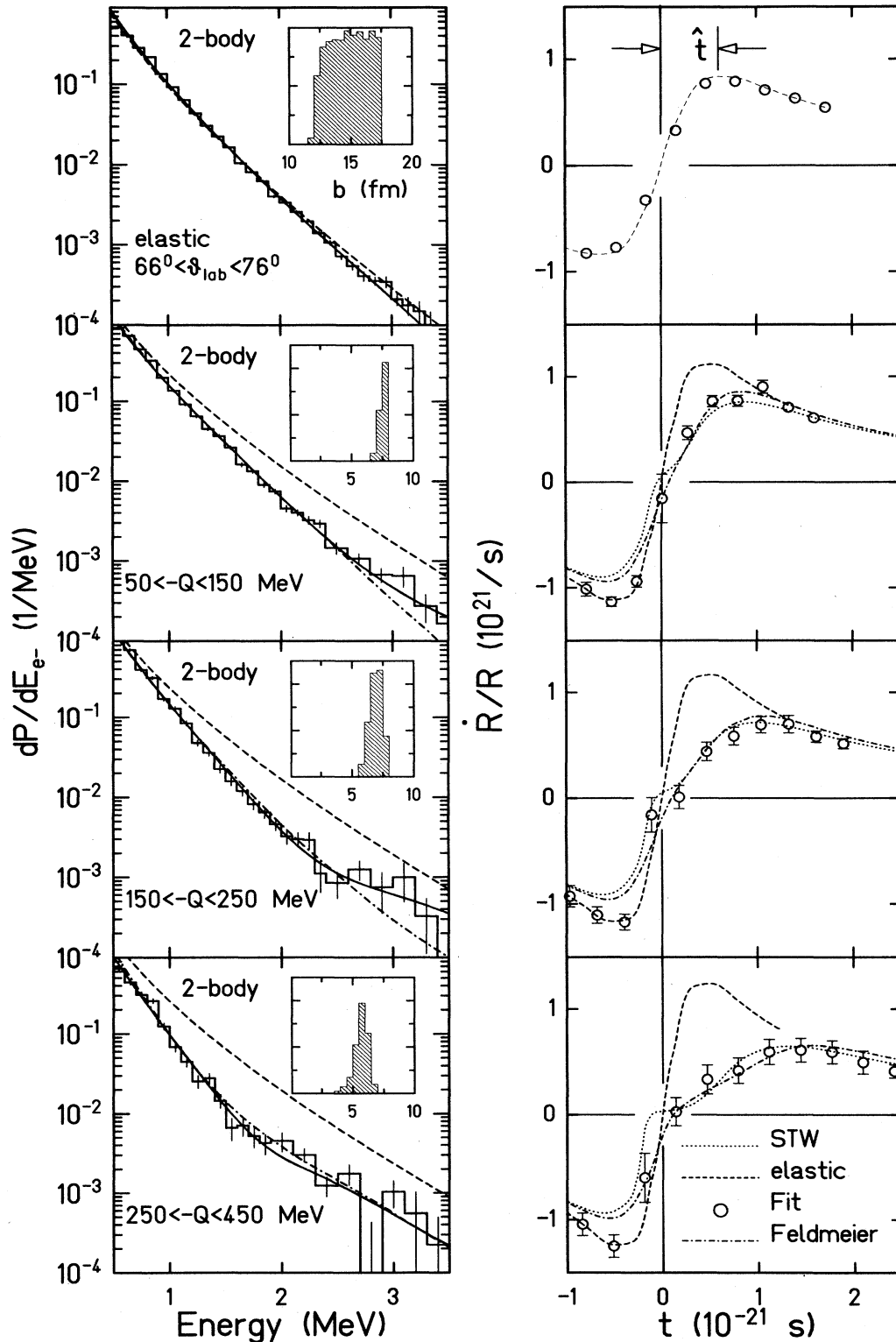


FIG. 12.  $\delta$ -electron spectra (left) and  $\dot{R}(t)/R(t)$  curves (right) using the fit procedure described in the text. Dashed: Rutherford trajectories; dash-dotted: Feldmeier trajectories; dotted: STW trajectories.

8.6 MeV/nucleon were measured in coincidence with three-body events with good  $Q$  resolution and energy losses up to 400 MeV using a different experimental device. Their findings agree with ours from binary collisions at similar  $Q$  values.

### C. Model-independent analysis of $\delta$ -electron spectra

In this section the direct extraction of information about the reaction dynamics from the  $\delta$ -electron spectra is discussed. The main idea was published in Ref. 18. We recall Eq. (1) stating that the transition amplitude is essentially the Fourier transform of the dynamic quantity  $\dot{R}(t)/R(t)$ . Because the  $\delta$ -electron spectra are obtained as the square of the amplitude the inverse transformation to directly yield  $\dot{R}(t)/R(t)$  is not possible. Our approach exploits the fact that only a small part of the whole trajectory  $\dot{R}(t)/R(t)$  is of interest. The integral in Eq. (1) can be divided into three parts:

$$\int_{-\infty}^{-3\hat{t}_{\text{in}}} dt \frac{\dot{R}}{R}(t) \exp(i\omega t) + \sum_{k=1}^m \Delta t_k \frac{\dot{R}}{R}(t_k) \exp(i\omega t_k) + \int_{3\hat{t}_{\text{out}}}^{\infty} dt \frac{\dot{R}}{R}(t) \exp(i\omega t), \quad (7)$$

with  $\omega = \Delta E/\hbar$ . The indices in and out refer to the kinematical parameters in the entrance and exit channel, respectively. Mean  $b$  values according to the impact parameter distributions (shown as insets in Fig. 12) were chosen. The average binding energy of electrons contributing to the spectra was adjusted to reproduce the coupled-channels calculations for elastic scattering. A value of 180 keV was adopted for Pb+Pb. Parts one and three were treated analytically using the approximations in Ref. 4:

$$\frac{\dot{R}}{R} \approx \frac{t}{t^2 + \hat{t}^2} \approx \frac{1}{t} \left[ 1 - \left( \frac{\hat{t}}{t} \right)^2 \right], \quad (8)$$

with the characteristic collision time

$$\hat{t} = (a/v)(\epsilon + 1.6 + 0.449/\epsilon). \quad (9)$$

Here,  $\epsilon$  is the eccentricity,  $2a$  the distance of closest approach, and  $v$  the projectile velocity for the entrance and exit channel, respectively. The second approximation in Eq. (8) is justified for  $|t| > 3\hat{t}$ .

The sum replaces the integral over the time region of interest and runs from  $t_k = -3\hat{t}_{\text{in}}$  to  $\hat{t}_k = 3\hat{t}_{\text{out}}$  with 12 equidistant time steps. The values of  $\dot{R}(t_k)/R(t_k)$  were allowed to vary in the range  $-t(R_{\text{interaction}}) < t_k < 3\hat{t}_{\text{out}}$  to fit the experimental data. The number of free parameters is limited by the number of data points available in the  $\delta$ -electron spectra ( $\approx 25$ ). An interaction radius  $R_{\text{interaction}}$  of 16 fm has been used. This time interval covers the dissipation phase as well as the deceleration in the entrance channel. Figure 12 shows the resultant  $\dot{R}(t)/R(t)$  values (symbol on the right-hand side) together with the calculated spectral distributions (solid curves on the left-hand side). The error bars of the fit results correspond to the experimental errors of the electron spectra. They are obtained from the curvature matrix of

the fit parameters.<sup>20</sup>

As there are free parameters both in the entrance as well as in the exit channel the result is not necessarily unique. In order to separate the influence of deceleration in the approaching phase from energy dissipation in the exit channel a different fit has been performed where the parameters are allowed to vary only in the range  $0 < t < 3\hat{t}_{\text{out}}$ . It turns out that the  $\dot{R}(t)/R(t)$  curves are quite similar in the range  $t > 0$ , so the inclusion of deceleration does not alter the result in the contact phase

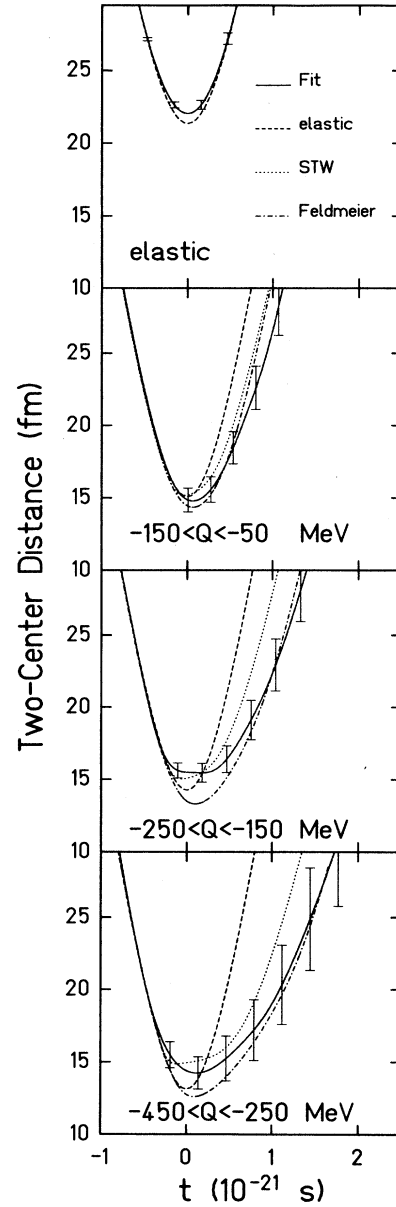


FIG. 13. Trajectories obtained by numerical integration of the  $\dot{R}(t)/R(t)$  curves. Solid line: numerical integration of fitted  $\dot{R}(t)/R(t)$  curve; dashed: Rutherford trajectory; dotted: two-center distance according to the STW model; dash-dotted: two-sphere center distance  $s$  according to the Feldmeier model.

significantly. One has to keep in mind that only limited information on the entrance channel can be extracted from  $\delta$ -electron spectra in the range up to 3 MeV. The time scale for deceleration is about  $10^{-22}$ s leading to Fourier frequencies which correspond to electron energies around 7 MeV.

At this point we emphasize that all trajectories have to be considered as “mean” trajectories. No fluctuations are

explicitly introduced in our fit procedure. However, the concept of a “mean” trajectory includes implicitly an averaging over a distribution of single trajectories.

Figure 12 (left-hand side) also represents the functions  $\dot{R}(t)/R(t)$  calculated within the scaling model using the STW model<sup>7</sup> (dotted curves) and the reaction model of Feldmeier<sup>8</sup> (dash-dotted curves). They mostly exhibit a good agreement with the experimental data in the exit

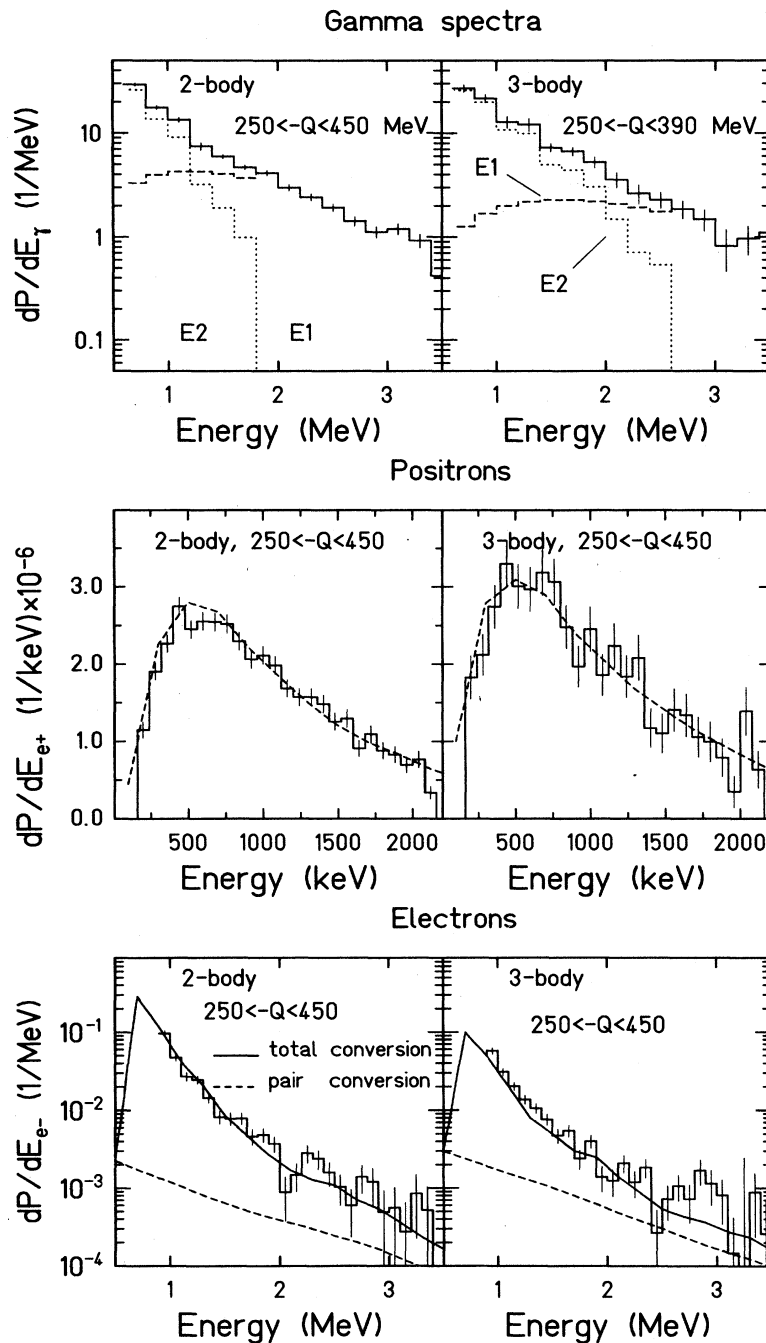


FIG. 14. Study of the reaction  $\text{Pb} + \text{Tm}$  at 8.4 MeV/nucleon. Upper part: measured  $\gamma$  spectra (solid histograms) together with the assumed multipolarity decomposition (E1, dashed E2, dotted). Middle part: measured positron spectra (histograms) with calculated nuclear positrons (dashed curve). The good agreement confirms the multipolarity assignment. Lower part: measured electron spectra (histograms) are exhausted by the calculated conversion contributions (solid and dashed curves).

channel. These calculations were carried out with the corresponding impact parameter distributions. The calculated spectra are shown in Fig. 11 (STW model) and Fig. 12 (Feldmeier model).

The  $\dot{R}(t)/R(t)$  values deduced by the fitting procedure are integrated to yield the trajectories  $R(t)$ . The integration constant is determined to match a Rutherford trajectory for  $t < -3\hat{t}_{in}$ . The resultant trajectories for the different  $Q$ -value windows are depicted in Fig. 13. As  $R(t)$  is a derived quantity the uncertainties of  $\dot{R}(t)/R(t)$  accumulate and lead to large error bars. The corresponding trajectories of the two reaction models are given, too. Up to now the symbol  $R$  refers to the rms radius of the dinuclear charge distribution. In Fig. 13 we have chosen to give the distance in a commonly used quantity, the distance between the centers of the two nuclei. It is used in the STW model which considers only spherical nuclei. For the Feldmeier model the quantity labeled  $s$  is presented which is the two-sphere center distance.<sup>8</sup>

A comparison between our fit procedure and the two models is best made by the  $\dot{R}(t)/R(t)$  curves due to the smaller errors (primary quantity), but is more familiar in the  $R(t)$  representation. Both reaction models predict too short nuclear contact for the peripheral collisions at impact parameters around 6–8 fm. For the highest energy loss ( $-450 < Q < -250$  MeV) they agree within the error bars. The Feldmeier model gives a better agreement with the data, at least for the considered electron energies below  $\approx 3$  MeV. This model treats the exit channel in a realistic way allowing for neck formation which leads to smooth shapes of the function  $\dot{R}(t)/R(t)$  and  $R(t)$ .

#### D. Medium-heavy systems

Because of their high nuclear charge the collision dynamics of the systems Pb+Pb and Pb+U are dominated by the large Coulomb repulsion. For lower charges the nuclear attraction becomes more important relative to the electromagnetic interaction and much longer contact times can be expected. For example, in the system Xe+Bi at 10 MeV/nucleon contact times up to  $10^{-20}$  s for central collisions were derived from an analysis of the deflection function.<sup>21</sup> Therefore, the feasibility of  $\delta$ -electron spectroscopy when investigating lighter systems was verified. Unfortunately, the production probability for  $\delta$  electrons decreases strongly with the combined nuclear charge and nuclear conversion may dominate the spectra.

As examples the systems Pb+Pd at 8.6 MeV/nucleon and Pb+Tm at 8.4 MeV/nucleon having a combined nuclear charge of  $Z_{united}$  of 128 and 151, respectively, were studied.

In analogy to the analysis of the Pb+Pb and Pb+U data windows were placed in the  $Q$ - $\vartheta$  distribution, and lepton as well as  $\gamma$  spectra were taken in coincidence to these windows. The  $\gamma$  spectra were decomposed into  $E1/E2$  multiplicities and converted into lepton spectra as discussed. The upper part of Fig. 14 shows the experimental  $\gamma$  spectra for the reaction Pb+Tm with assumed  $E1/E2$  decomposition. For three-body events an en-

larged contribution of  $E2$  multipolarity at  $\gamma$  energies around 2 MeV is needed. This seems reasonable because the level schemes of the nuclei in the Pd region indicate many  $E2/M1$  transitions.<sup>22</sup> Further on, this result is analogous to the findings in three-body events of Pb+Pb where also nuclei in the Nb-Pd region are created. With the indicated  $E1/E2$  mixtures the measured positron spectra are reproduced by the calculated nuclear pair conversion (middle part of Fig. 14). A reduction of the  $E2$  multipolarity in favor of the  $E1$  part would lead to an overestimation of the positron yield. The electron spectra deduced from nuclear conversion exhaust the measured ones, too. Hence, the system Pb+Tm is not accessible for  $\delta$ -electron spectroscopy at this  $Q$  value. At a  $Q$  value around  $-100$  MeV a surplus of about 50% remains in the electron spectra. The measured positron and electron spectra of the collision system Pb+Pd at 8.6 MeV/nucleon can be reproduced quantitatively by conversion from the  $\gamma$  spectra at all  $Q$  values.

The results for the production probabilities of electrons in the energy range  $1050 < E_{e^-} < 1500$  keV which are the most sensitive to time delay, are summarized in Fig. 15 as a function of the combined nuclear charge for binary col-

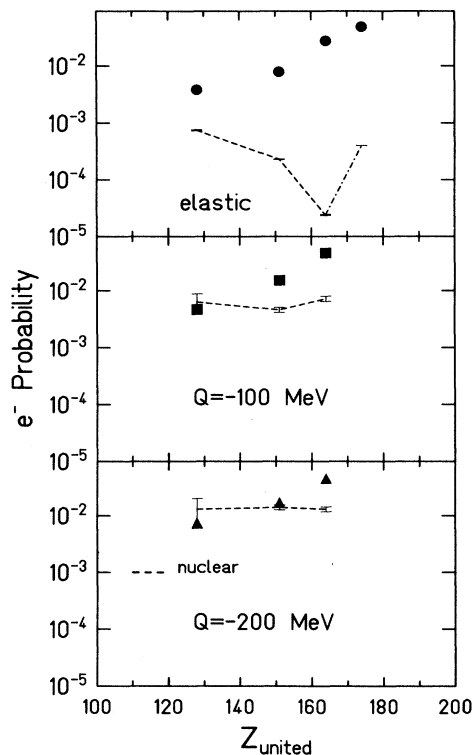


FIG. 15. Electron production probabilities  $P_{e^-}$  for various  $Q$  values. The integrated probabilities in the range  $1050 < E_{e^-} < 1500$  keV for binary collisions are plotted versus the combined nuclear charge. At least one collision partner is Pb, the bombarding energies are around 8.5 MeV/nucleon. The points for elastic scattering were chosen for the characteristic collision time of  $2\hat{t} \approx 1 \times 10^{-21}$  s. The dashed curves represent the probability for conversion electrons as calculated from the  $\gamma$  spectra.

lisions at various  $Q$  values. The comparison with the calculated nuclear contribution allows an estimation of the lower limit of  $\delta$ -electron spectroscopy in deep-inelastic reactions. Depending on the  $Q$  value, it is located within  $130 < Z_{\text{united}} < 155$ . These findings might be limited to bombarding energies around 8.5 MeV/nucleon.

The  $\delta$ -electron production probability for elastic scattering scales roughly with the density of the  $1s\sigma$  wave function at the origin of the combined system<sup>4</sup> and coincides for  $Z_{\text{united}} < 100$  with the probability for conversion electrons.

## V. SUMMARY AND CONCLUSIONS

The analysis of  $\delta$ -electron spectra from dissipative reactions of the systems Pb+U and Pb+Pb are presented as a tool to deduce the collision dynamics. For these systems with a combined nuclear charge  $Z_{\text{united}} \leq 174$  the simultaneous measurement of the positrons allows one to verify the multipolarity assignment (only  $E1/E2$ ) of the  $\gamma$  transitions above 1 MeV. This is essential for a precise determination of electrons from conversion.

The  $\delta$ -electron spectra clearly show the expected influence of nuclear contact. A broad minimum at electron energies around 1.5–2 MeV is seen becoming more pronounced with increasing energy loss. Deviations from coupled-channels calculations for some subgroups of the reaction Pb+U are interpreted as indications of fluctuations in the contact time  $\tau$ . A model-dependent estimate

yields  $\Delta\tau/\tau \approx 1$ .

The main information is obtained from an analysis of the  $\delta$ -electron spectra independent of nuclear models allowing us to determine  $\dot{R}(t)/R(t)$  curves and the trajectories  $R(t)$  of dissipative collisions. They are compared with two reaction models. For peripheral collisions ( $-50 \leq Q \leq -250$  MeV) generally longer nuclear contact is found. At the highest energy loss the model of Feldmeier describes the data best.

Finally, a lower limit for the applicability of  $\delta$ -electron spectroscopy with the present technique is shown. The analysis of  $\delta$ -electron spectra does not seem to be feasible due to the overwhelming conversion contribution in the electron spectra for  $Z_{\text{united}} < 130-155$ , depending on the  $Q$  value.

## ACKNOWLEDGMENTS

We would like to thank S. Graf and Th. de Reus from the University of Frankfurt for performing the coupled-channels calculations. The preparations of the targets by H. Folger and the GSI target laboratory and the construction of dedicated electronic units by J. Foh and the electronic workshop of the Institut für Kernphysik, Darmstadt is gratefully acknowledged. This work is supported by the Bundesministerium für Forschung und Technologie under Contract 06DA453 and by the Gesellschaft für Schwerionenforschung, Darmstadt.

\*Present address: Gesellschaft für Schwerionenforschung mbH, D 6100 Darmstadt, Federal Republic of Germany.

†Permanent address: Institute of Nuclear Physics, Cracow, Poland.

<sup>1</sup>H. Backe, P. Senger, W. Bonin, E. Kankeleit, M. Krämer, R. Krieg, V. Metag, N. Trautmann, and J. Wilhelmy, *Phys. Rev. Lett.* **50**, 1838 (1983).

<sup>2</sup>R. Krieg, E. Bozek, U. Gollerthan, E. Kankeleit, G. Klotz-Engmann, M. Krämer, U. Meyer, H. Oeschler, and P. Senger, *Phys. Rev. C* **34**, 562 (1986).

<sup>3</sup>Ch. Stoller, M. Nessi, E. Morenzoni, W. Wölfl, W. E. Meyerhoff, J. D. Molitoris, E. Grosse, and Ch. Michel, *Phys. Rev. Lett.* **53**, 1329 (1984).

<sup>4</sup>E. Kankeleit, *Nukleonika* **25**, 253 (1980).

<sup>5</sup>E. Kankeleit, *International Advanced Courses on Physics of Strong Fields*, edited by W. Greiner (Plenum, New York, 1987), p. 359.

<sup>6</sup>G. Soff, J. Reinhardt, B. Müller, and W. Greiner, *Phys. Rev. Lett.* **43**, 1981 (1979); U. Müller, G. Soff, J. Reinhard, T. de Reus, B. Müller, and W. Greiner, *Phys. Rev. C* **30**, 1199 (1984).

<sup>7</sup>R. Schmidt, V. Toneev, and G. Wolschin, *Nucl. Phys.* **A311**, 247 (1978); G. Wolschin, *Nukleonika* **22**, 1165 (1977).

<sup>8</sup>H. Feldmeier, in *Nuclear Structure and Heavy-Ion Dynamics, LXXXVII Corso Bologna*, edited by L. Moretto and R. Ricci (North-Holland, Amsterdam, 1984).

<sup>9</sup>E. Kankeleit, U. Gollerthan, G. Klotz, M. Kollatz, M. Krämer, R. Krieg, U. Meyer, H. Oeschler, and P. Senger, *Nucl. Instrum. Methods* **A234**, 81 (1985).

<sup>10</sup>P. Glässel, D. V. Harrach, H. J. Specht, and L. Grodzins, *Z. Phys. A* **310**, 189 (1983).

<sup>11</sup>S. Graf, J. Reinhardt, U. Müller, T. de Reus, B. Müller, W.

Greiner, and G. Soff, *Z. Phys. A* **329**, 365 (1988).

<sup>12</sup>M. Krämer, Ph. D. thesis, Institut für Kernphysik, TH Darmstadt, 1988.

<sup>13</sup>G. Wolschin, in *Nuclear Structure and Heavy-Ion Collisions, LXXVII Corso Varenna*, edited by R. A. Broglia, R. A. Ricci, and C. H. Dasso (North-Holland, Amsterdam, 1981).

<sup>14</sup>T. Tanabe, R. Bock, M. Dakowski, A. Gobbi, H. Sann, H. Stelzer, U. Lynen, A. Olmi, and D. Pelte, *Nucl. Phys.* **A342**, 194 (1980).

<sup>15</sup>P. Schlüter, G. Soff, and W. Greiner, *Phys. Rep.* **75**, 327 (1981); Institut für Theoretische Physik, Universität Frankfurt am Main Report 10/1980, 1980.

<sup>16</sup>R. S. Hager and E. C. Seltzer, in *Atomic and Nuclear Data Reports, Internal Conversion Coefficients*, edited by Katharine Way (Academic, New York, 1973); V. F. Trusov, *ibid.*

<sup>17</sup>M. Krämer, B. Blank, E. Bozek, E. Kankeleit, G. Klotz-Engmann, C. Müntz, H. Oeschler, and M. Rhein (unpublished).

<sup>18</sup>M. Krämer, B. Blank, E. Bozek, E. Kankeleit, G. Klotz-Engmann, C. Müntz, H. Oeschler, and M. Rhein, *Phys. Lett. B* **201**, 215 (1988).

<sup>19</sup>P. Senger, H. Backe, M. Begemann-Blaich, H. Bokemeyer, P. Glässel, D. V. Harrach, M. Klüver, W. Konon, K. Poppensieker, K. Stiebing, J. Stroth, and K. Wallenwein, in *International Advanced Courses on Physics of Strong Fields*, edited by W. Greiner (Plenum, New York, 1987), p. 423.

<sup>20</sup>Ph. R. Bevington, *Data Reduction and Error Analysis for the Physical Sciences* (McGraw-Hill, New York, 1969).

<sup>21</sup>H. J. Wollersheim, W. W. Wilcke, J. R. Birekelund, and J. R. Huizenga, *Phys. Rev. C* **25**, 338 (1982).

<sup>22</sup>C. M. Lederer and V. S. Shirley, *Table of Isotopes*, 7th ed. (Wiley, New York, 1978).